JPE 8-1-6

Three-Phase AC-to-DC Resonant Converter Operating in High Power Factor Mode in High-Voltage Applications

Madhuri A. Chaudhari[**], Hiralal M. Suryawanshi[†], Abhishek Kulwal[*] and Mahesh K. Mishra[***]

[†*]Electrical Engineering Department, Visvesvaraya National Institute of Technology, India
[**]Electrical Engineering Department, Yeshwantrao Chavan College of Engineering, India
[***]Electrical Engineering Department, Indian Institute of Technology, India

ABSTRACT

In this paper a three-phase ac-to-dc resonant converter with high input power factor and isolated output is proposed. To improve the input power factor of the converter, high frequency current is injected into the input of the three-phase diode bridge rectifier. It is injected through an impedance network consisting of a series of *L*-*C* branches from the output of the high frequency three-phase inverter. A narrow switching frequency variation is required to regulate the output voltage. A design example with different design curves is illustrated along with the component ratings. Experimental verification of the converter is performed on a prototype of 3 kW, 1000 V output, operating above 300 kHz. Experimental results confirm the concept of the proposed converter. Narrow switching frequency variation is required to regulate the output voltage.

Keywords: High frequency current injection, ac-to-dc resonant converter, power factor, zero-voltage switching, voltage and current stresses

1. Introduction

Resonant converters are now used in many power applications. This is because of their higher frequency operation, smaller size, lighter weight, reduced electromagnetic interference, relatively higher efficiency and better dynamic response compared to pulse width modulation based converters. Further, by proper design and selection of the resonant tank elements, switching losses can be reduced drastically [1]-[7]. In [1]-[3], high power factor operation of the resonant converter is presented, but the converters are also useful for single-phase ac-to-dc applications. The advantages of the three-phase dc-to-dc resonant converter are given in [4] and [5]. A three-phase dc-to-dc resonant converter can be used in high power applications. It reduces output and input ripples allowing small filter components and requires narrow variation in switching frequency to control the output power. The high power factor three-phase converter presented in [6] is based on a single-phase dc-to-dc resonant converter, which is useful for low power applications. In [7], the three-phase dc-to-dc resonant converter is used in single-phase applications. For high power factor operation of the three-phase converter, many schemes such as the active power filter (APF) and third harmonic current injection method [8]-[10] are presented. These schemes suffer from the following drawbacks: active devices in the inverter are hard switched; the load side is not isolated from the supply side; they require a line synchronized and controllable external third harmonic

Manuscript received Sep. 3, 2007; revised Nov. 23, 2007
[†]Corresponding Author: hms_1963@ rediffmail.com
Tel: +91-712-2801122, Fax: +91-712-2223230, V.N.I.T., India
[*]Electrical Engineering Department, V.N.I.T., India
[**]Yeshwantrao Chavan College of Engineering, India
[***]Electrical Engineering Department, I.I.T., India

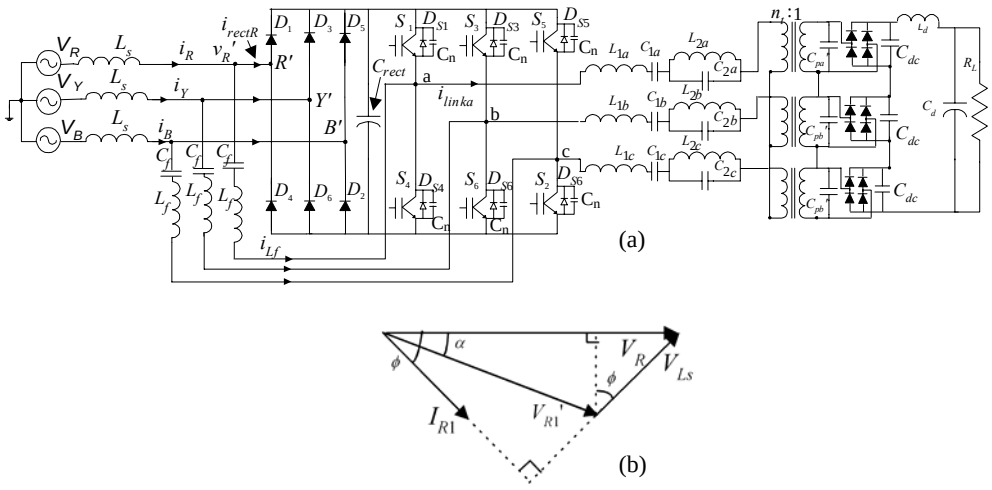

Fig. 1 (a) Circuit diagram of three-phase ac-to-dc resonant converter
(b) Phasor diagram of the converter at fundamental frequency

current source; and the tuned third harmonic filter draws excessive fundamental current. In [6] efficiency is reported as 85% and THD is reported as 6%. In [8] and [9] THD is reported as 4.5% and 12%, respectively. In [11], the power factor improvement of the three-phase supply using high frequency current injection with a zero-voltage switching (ZVS) topology is presented. It has drawbacks such as: it is based on a half bridge inverter; to achieve a high modulation index, the resonant current must be three times the line current. This limits the circuit application to low power ranges.

This paper presents a three-phase ac-to-dc resonant converter operated in high power factor mode for high voltage dc applications. This configuration is based on the high frequency (HF) current injection method. HF current is injected into the input of the three-phase input diode bridge rectifier, thereby producing HF modulation of the rectifier input voltage. It uses a three-phase full-bridge HF inverter with a modified series-parallel resonant load (MSPRC) [7]. Thus, the proposed converter has all the advantages of the resonant converter as discussed above with the additional advantages of a three-phase dc-to-dc resonant converter [4]. This paper deals with the analysis and design of the proposed converter. MATLAB subroutines are developed to plot the different design curves. A design example is outlined along with the component ratings. Experimental results are presented to confirm the concept and design of the proposed converter.

2. Operation of the Converter

Fig. 1(a) shows the proposed three-phase ac-to-dc resonant converter and Fig. 1(b) shows the phasor diagram of the ac input side of the converter. The proposed three-phase ac-to-dc resonant converter consists of supply inductors L_s, a three-phase diode bridge rectifier, a small dc link capacitor C_{rect}, a three-phase dc-to-dc modified series-parallel resonant converter (MSPRC), and a HF current injection network. The MSPRC consists of a three-phase HF inverter with a three-phase resonant tank circuit followed by a HF transformer, rectifier and load. The three-phase resonant tank consists of L_1, L_2, C_1, C_2 and C_p in all three phases. These components in the three phases have been denoted by subscripts a, b and c, respectively. Three single-phase HF transformers are used to isolate the load from the input supply and to obtain the desired level of the output voltage. In Fig. 1(a), the C_p is placed on the secondary side of the HF transformer to include the leakage inductance of the HF transformer into the resonant inductor L_1. Thus, the actual value of the externally required resonant inductor is reduced in the tank circuit. The converter is designed for 1000 V output dc application. To reduce the voltage stress, switching and

conduction loss in the diodes of the output bridge rectifier, three single-phase diode-bridge rectifiers are connected in series at the output HF transformer. The output filter inductor (L_d) is designed to remove the six time switching frequency ripples of the output current, and the capacitor (C_d) is designed to remove the six time supply frequency ripples of the output voltage. Hence, the filtering requirement is drastically reduced. The HF current injection network is comprised of a set of inductor L_f and capacitor C_f. HF current is injected from the three-phase HF inverter into the input of the three-phase diode bridge rectifier. Hence, the frequency of the HF injected current is the same as that of the frequency of the operation of the HF inverter. The HF inverter is operated on a 180^0 wide gating control scheme. Hence, at any instant, three switches, one from each leg, remain in conduction. The MSPRC tank circuit is designed at resonance frequency (ω_r). Therefore, the inverter line current (link current) will be in phase with the fundamental component of the output phase voltage. To regulate the output voltage and to achieve ZVS, the proposed three-phase resonant converter is operated above the resonant frequency. Hence, the fundamental component of the link current lags behind the phase voltage. This causes conduction of the anti-parallel diode before the conduction of the semiconductor power device (IGBT) of the HF inverter. Therefore, at the instant of turn-on of the IGBT, voltage across the IGBT is equal to the forward voltage drop across the anti-parallel diode. This voltage drop will be negligible. Thus, zero voltage switching (ZVS) turn-on of all the switches of the HF inverter is achieved. This reduces the turn-on losses of the HF inverter. Connecting a small, loss-less snubber capacitor across each switch of the HF inverter can minimize the turn-off losses. Due to a small snubber capacitor (C_n), the transition period of the IGBTs compared to the switching period T_s is negligible. This facilitates the HF operation of the inverter.

The input supply current is the instantaneous sum of the HF injected current (i_{Lf}) and the input current of the input diode bridge rectifier. HF current injection produces HF modulation of the input voltage of the diode bridge rectifier. The HF modulated input voltage of the diode bridge rectifier has a sinusoidal PWM pattern. This HF PWM pattern of the voltage forces the upper diode on the leg of the diode bridge rectifier to turn on and off in positive cycle at the rate of frequency modulation index m_f, where m_f is the ratio of the switching frequency of the HF inverter to the input supply frequency. Similarly, the lower diode on the leg of the input diode bridge rectifier turns on and off in negative cycle of the input supply voltage at the rate of frequency modulation index m_f. Fig. 2(a) shows the theoretical waveforms of the input supply current (i_R), input diode current (i_{D1}) and HF injected current (i_{Lf}) in positive cycle of the supply voltage. The high switching frequency of the inverter as compared to the supply frequency results in forceful conduction of the diodes over the complete cycle of the input supply voltage including valley points. Thus, continuous current conduction mode (CCM) of the supply inductor L_s is obtained. Hence, inherent improvement of the input power factor can be achieved. Due to the HF modulation of the input voltage to the input diode bridge rectifier, the input diodes are operated in discontinuous current conduction mode.

The current through the input diode is a triangular waveform. In the HF current injection branch the inductive reactance of L_f is greater than the capacitive reactance of C_f, hence the HF injected current is also a triangular waveform. triangular waveform. The main power circuit shown in Fig. 1(a) passes through 12 different modes of operation in one switching cycle of the HF inverter. These modes are defined by the switching sequence of the devices of the HF inverter. During the positive cycle of the link current (inverter line current), i.e. when the upper IGBT on the leg is in conduction, the current through the feedback inductance L_f decreases from its positive peak (I_{Lfp}) to its negative peak ($-I_{Lfp}$) as shown in Fig. 2(b). Thus, in the time period $T_s/2$, change in the injected current is $2I_{Lfp}$ and voltage across L_f is held constant at -V_{rect}/2, which is approximately equal to the peak value of the supply voltage. During this time period $T_s/2$, the input diode current increases linearly from zero to its maximum value. The L_f releases its energy in the first $T_s/4$ period and in the next $T_s/4$ period it restores energy in the opposite direction. When L_f fully releases its energy the current through it becomes zero and the input diode current

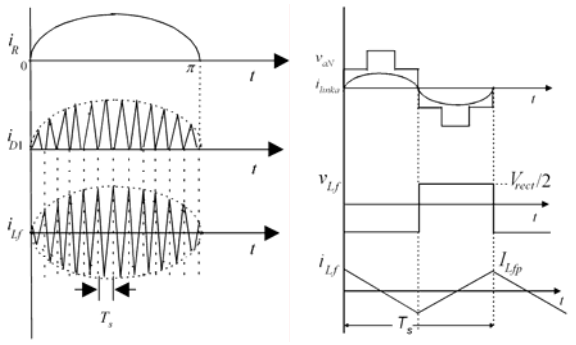

(a) (b)

Fig. 2 (a) Operating waveforms (During positive cycle of v_R) Input current (i_R), diode current (i_{D1}), HF injected current (i_{Lf}). (b) Output phase voltage (v_{aN}) and phase current (i_{linka}) of the HF inverter, Voltage across L_f(v_{Lf}), current through L_f (i_{Lf}) in one switching cycle of the HF inverter

becomes equal to the supply current. In the negative cycle of the link current, i.e. when the lower device on the leg is in conduction, the current through the feedback inductance L_f increases from its negative peak $(-I_{Lfp})$ to its positive peak (I_{Lfp}), and the input diode current decreases from its maximum value to zero. During this period the voltage across L_f is held constant at $+V_{rect}/2$. The capacitor C_f provides dc blocking to the HF injected current. Hence, the capacitor C_f should be sufficiently large so that voltage across it is held at $V_{rect}/2$ throughout the switching cycle, which is approximately equal to the peak of the supply voltage.

The peak values of the HF injected current and diode current vary over the cycle of the input supply voltage. The peak values depend on the instantaneous value of the input supply current. At the peak of the input supply voltage, the peak value of the HF injected current is the same as peak of the input supply current. For proper operation of the converter, which allows full reset of the diode current, the minimum dc link voltage, V_{rect} (voltage across C_{rect}) must be twice the maximum value of the supply phase voltage.

2.1 AC input line current

The balanced three-phase input supply phase voltages are given by,

$$v_R = V_m \sin \omega t, v_Y = V_m \sin(\omega t - \frac{2\pi}{3}), v_B = V_m \sin(\omega t + \frac{2\pi}{3}) \quad (1)$$

In the absence of a neutral connection to the bridge rectifier, the sum of ac currents must be equal to zero at all times.

$$i_R + i_Y + i_B = 0 \quad (2)$$

It also applies to the derivative of the sum of the alternative currents. The input supply current is as,

$$i_R = i_{LfR} + i_{rectR}, \quad i_Y = i_{LfY} + i_{rectY}, \quad i_B = i_{LfB} + i_{rectB} \quad (3)$$

where $i_{LfR}, i_{LfY}, i_{LfB}$ are HF injected currents and $i_{rectR}, i_{rectY}, i_{rectB}$ are input currents of the three-phase diode bridge rectifier. If v_R' is the input voltage to the input diode bridge rectifier, then the input current through the supply inductor is,

$$i_R = \frac{v_R - v_R'}{jX_{L_s}} \quad (4)$$

The supply voltages described by (1) contain only the fundamental component. Hence, in order for the harmonic content in the supply current to exist, the supply must act as a short circuit for these harmonic currents. The harmonic current components are then solely determined by the harmonic voltage of the input voltage to the diode bridge rectifier [12]. The HF injected current produces HF modulation of the input voltage to the diode bridge rectifier. The HF modulated voltage v_R' has a HF sinusoidal PWM pattern, analogous to a unipolar voltage switching scheme. This scheme has the advantage of effectively 'doubling' the switching frequency as far as the harmonics are concerned [13]. Since the switching frequency is very high, a small L_s can filter out the sets of switching frequency sideband present in the input supply current due to v_R'. Fig. 1(b) shows the phasor diagram of the ac input side of the converter. The phasor diagram

includes the ac source voltage V_R, the voltage across supply the inductor V_{Ls}, and the fundamental component V_{R1}' of v_R'. The angle α is the phase shift angle between V_R and V_{R1}'. Therefore, the fundamental component of the input line current is given by [13],

$$I_{R1}\angle\phi = \frac{V_R - V_{R1}'\angle\alpha}{jX_{Ls}} \tag{5}$$

The real power transfer to the rectifier,

$$P_i = \frac{V_R \cdot V_{R1}'}{X_{Ls}} \cdot \sin\alpha \tag{6}$$

From (5), the magnitude of the fundamental component of the input line current and the power factor angle ϕ are given by,

$$|I_{R1}| = \sqrt{\left((V_R - V_{R1}'\cos\alpha)^2 + (V_{R1}'\sin\alpha)^2\right)/\left(jX_{Ls}\right)^2} \tag{7}$$

$$\phi = \tan^{-1}\frac{V_R - V_{R1}'\cos\alpha}{V_{R1}'\sin\alpha}$$

$$pf = \cos\phi = \frac{V_{R1}'\cdot\sin\alpha}{\sqrt{V_R{}^2 + V_{R1}{}'^2 - 2\cdot V_R\cdot V_{R1}'\cdot\cos\alpha}} \tag{8}$$

From (7) and (8), it is clear that for the given supply voltage and the selected source inductor, the magnitude of the fundamental component of the input line current and the power factor angle ϕ can be controlled by controlling the v_R'. To limit the ripples in input line current and to obtain high power factor, the converter is pulse width modulated at high switching frequency in the linear region of modulation index ($m = V_p/(V_{rect}/2)$). This results in line-to-line input voltage to the diode bridge rectifier [14] as,

$$V_{LL(rms)} = \frac{\sqrt{3}}{2\sqrt{2}}\cdot m\cdot V_{rect} \qquad (m \le 1.0)$$

$$V_{rect} = 2\cdot V_m \tag{9}$$

Due to the HF current injection, the input diodes are operated in discontinuous current mode. The diode current is a triangular waveform. The above value of V_{rect} also ensures the proper resetting of the input diode current.

A constant β is defined as,

$$\beta = \frac{\sqrt{2}\,V_{R1}'}{\sqrt{2}\,V_R} \tag{10}$$

From (8) and (10),

$$\phi = \tan^{-1}\frac{V_R{}^2 - \sqrt{\beta^2\cdot V_R{}^4 - P_i{}^2\cdot X_{Ls}{}^2}}{P_i.X_{Ls}} \tag{11}$$

The variation of power factor with respect to input power for various values of β is studied. These plots are studied for different values of X_{Ls}. Study of these plots shows that when $\beta \neq 1$, a high *pf* can be obtained at a particular value of P_i and not for any value of P_i. β =1 maintains the high *pf* throughout the loading conditions, i.e. at any value of P_i, with a selected value of X_{Ls}.

From (6) and (8), *pf* in terms of P_i and X_{Ls} when $V_R = 1\,pu$, is given by,

$$pf = \frac{P_i\cdot X_{Ls}}{\sqrt{2 - 2\sqrt{1 - P_i{}^2\cdot X_{Ls}^2}}} \tag{12}$$

The variation of *pf* with respect to P_i for different values of X_{Ls}, is plotted in Fig. 3(a) using MATLAB. These graphs suggest that at a lower value of X_{Ls}, input *pf* is high and varies between 1 and 0.995 for changes in power 0 to 1 *pu*. A smaller X_{Ls} implies a higher switching frequency. Hence, a high switching frequency of 300 kHz is selected. Hence, high power factor operation is achieved by using a small X_{Ls} and high switching frequency. Fig. 3(b) shows the variation of the angle α with respect to P_i, for different values of X_{Ls}. From this graph, it is clear that for lower values of X_{Ls} the angle α is very small. That means with a small value of X_{Ls}, V_{R1}' and v_R are almost in phase. Thus, with HF current injection and a small source inductor, high power factor operation of the converter is achieved.

2.2 HF current injection inductor, L_f

High power factor operation of the converter depends on HF current injection which is, in turn, decided by the HF current injection inductor L_f. HF current injection increases with a decrease in L_f. In this section the value of L_f required to maintain high power factor is decided. Equating the volt-second area of the current and voltage waveforms (i_{Lf}) and (v_{Lf}), shown in Fig. 2(b), over the switching time period (T_s),

$$I_{LfP} = \frac{V_{rect}}{2L_f} \cdot d^2 T_s \tag{13}$$

where d is the duty ratio. Referring to Fig. 2(a) and equation (3), when $i_{rectR} = i_{D1} = 0$, $I_{LfP} = i_R = I_m \sin \omega t$, therefore, equation (13) gives,

$$L_f = \frac{V_{rect}}{2 \cdot I_m \sin \omega t} \cdot d^2 T_s \tag{14}$$

The average three-phase input power over one cycle,

$$P_i = \frac{3}{\pi} \int_0^{\pi} v_R \cdot i_R \, d(\omega t) = \frac{3}{2} V_m \cdot I_m \tag{15}$$

Substituting I_m in terms of P_i and using (9), equation (14) gives

$$L_f = \frac{3}{2} \frac{V_m{}^2}{P_i \sin \omega t} \cdot d^2 T_s = \frac{3}{2} \frac{V_m{}^2 \cdot \eta}{P_0 \sin \omega t} \cdot d^2 T_s \tag{16}$$

where η is efficiency. The variation of L_f with respect to ωt shows that L_f is lowest at the peak of input voltage. Loading of the converter has maximum value at the peak of input supply; hence, design of L_f is carried out at the peak of supply voltage, i.e. at $\omega t = \pi / 2$. Hence, from (16),

$$L_f = \frac{3}{2} \cdot \frac{d^2 T_s \eta V_m{}^2}{P_0} \tag{17}$$

Fig. 3(c) and Fig. 3(d) show the variation of L_f with the duty ratio and input supply peak voltage under different loading conditions. From Fig. 3(c) it can be seen that to regulate the output voltage with the designed value of L_f, the duty ratio has to be reduced. The variation of the duty ratio required is about 40% over the load range of full load to 25% of load. Similarly, from Fig. 3(d), it is clear that to

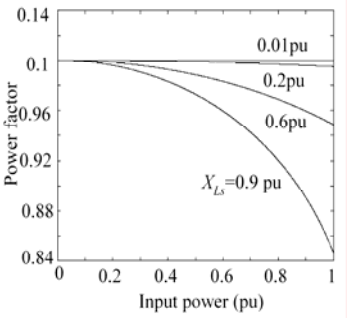

(a)

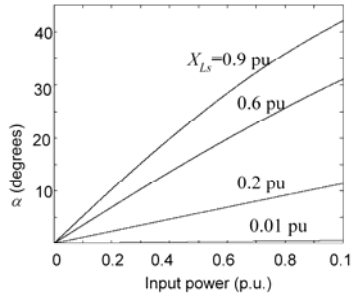

(b)

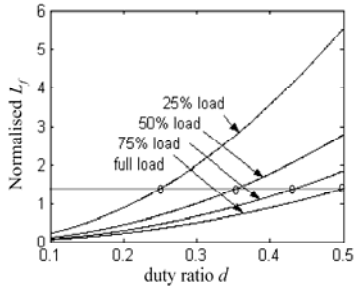

(c)

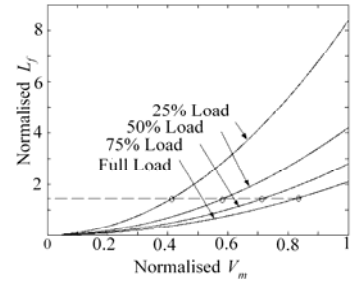

(d)

Fig. 3 (a) Variation of power factor with the per unit input power for various values of X_{Ls} (b) Variation of phase angle of $V_{R1}'(\alpha)$ with the per unit input power for various values of X_{Ls} (c) Variation of normalised L_f with the duty ratio d (d) Variation of normalised L_f with the normalized input peak voltage V_m

regulate the output voltage with the designed value of L_f under different loading conditions, the input voltage should be reduced. Circles on the graphs indicate operating points.

The output voltage of the converter is regulated by decreasing the input voltage to the HF transformer. This is achieved by increasing the switching frequency of the operation of the inverter and keeping the input voltage to the converter constant.

3. AC Analysis of the Proposed Circuit

3.1 Expressions of the voltage and current for the MSPRC tank

The output phase voltage of the HF inverter can be expressed in terms of a Fourier series [15] and is given by (19). For nth harmonics, the HF inverter output current is represented by equation (20), where θ_n is the phase angle of Z_{eq} for the nth harmonic. The Z_{eq} is the per phase equivalent load impedance for the HF inverter and it is given by,

$$Z_{seriesn} = jnX_{L1} - j\frac{1}{n}X_{C1} - \frac{jnX_{L2}\cdot j\frac{1}{n}X_{C2}}{jnX_{L2} - j\frac{1}{n}X_{C2}}$$

$$Z_{paralleln} = -j\frac{1}{n}X_{Cp}R_{ac}\Big/(R_{ac} - j\frac{1}{n}X_{Cp})$$

$$Z_{eqn} = Z_{seriesn} + Z_{paralleln} \quad (18)$$

$$v_{aN} = \sum_{n=1,5,7.....}^{\infty}\frac{2V_{rect}}{n\pi}\cdot\sin\left(\frac{n\delta}{2}\right)\cdot\sin\left(\frac{n\pi}{2}\right)\cdot\sin n(\omega_s t) \quad (19)$$

where δ is the pulse width of the gate voltage applied to the HF inverter switching devices and it is given by, $\delta = (1-d)\cdot 2\pi$ and ω_s is the switching frequency in rad/sec.

$$i_{linka} = \sum_{n=1,5,7.....}^{\infty}\frac{2V_{rect}}{n\pi|Z_{eqn}|}\sin\left(\frac{n\delta}{2}\right)\cdot\sin\left(\frac{n\pi}{2}\right)\cdot\sin(n\omega_s t - \theta_{eqn}) \quad (20)$$

The expressions for other phase voltages and link currents can be written using (19) and (20), respectively, with a phase shift of 120^0. The Fourier series expressions for the output line voltages of the HF inverter are written in (21), using equation (19), as

$$v_{ab} = \sum_{n=1,5,7.....}^{\infty}\frac{4V_{rect}}{n\pi}\sin\left(\frac{n\delta}{2}\right)\cdot\sin\left(\frac{n\pi}{2}\right)\cdot\cos\left(\frac{n\pi}{6}\right)\cdot\sin n\left(\omega_s t + \frac{\pi}{6}\right) \quad (21)$$

The other line voltages, v_{bc} and v_{ca} can be expressed using (21) with a phase shift of 120^0. Instantaneous voltage stresses over the series elements (L_1, C_1, L_2, C_2) of the MSPRC are derived from the expression for the link current (20), and are given by,

$$v_{L1} = \sum_{n=1,5,7.....}^{\infty}\frac{2V_{rect}\cdot X_{L1n}}{n\pi|Z_{eqn}|}\cdot\sin\left(\frac{n\delta}{2}\right)\cdot\sin\left(\frac{n\pi}{2}\right)\cdot\cos(n\omega_s t - \theta_{eqn})$$

$$v_{C1} = \sum_{n=1,5,7.....}^{\infty} -\frac{2V_{rect}\cdot X_{C1n}}{n\pi|Z_{eqn}|}\cdot\sin\left(\frac{n\delta}{2}\right)\cdot\sin\left(\frac{n\pi}{2}\right)\cdot\cos(n\omega_s t - \theta_{eqn})$$

$$v_{C2} = \sum_{n=1,5,7.....}^{\infty}\frac{2V_{rect}\cdot X_{L2C2n}}{n\pi|Z_{eqn}|}\cdot\sin\left(\frac{n\delta}{2}\right)\cdot\sin\left(\frac{n\pi}{2}\right)\cdot\cos(n\omega_s t - \theta_{eqn})$$

$$v_{L2} = v_{C2} \quad (22)$$

where, X_{L1}, X_{C1} are the reactances of the series elements, L_1 and C_1, and X_{L2C2} is the equivalent reactance of the parallel combination of L_2 and C_2.

The instantaneous voltage of the primary winding of the HF transformer can be expressed using the expression for the output phase voltages of the inverter (19). It is given by (23), where γ is the phase angle between the fundamental component of the HF inverter output phase voltage and the HF transformer primary winding voltage.

$$v_{prim} = \sum_{n=1,5,.....}^{\infty}\frac{2V_{rect}}{n\pi}\sin\left(\frac{n\delta}{2}\right)\sin\left(\frac{n\pi}{2}\right)\sin(n\omega_s t - \gamma_n) \quad (23)$$

The current through the capacitor C_p can be derived from the primary voltage of the transformer and is given by,

$$i_{Cp} = \sum_{n=1,5,.....}^{\infty}\frac{2V_{rect}}{n\pi\cdot X_{Cpn}}\sin\left(\frac{n\delta}{2}\right)\sin\left(\frac{n\pi}{2}\right)\cos(n\omega_s t - \gamma_n) \quad (24)$$

3.2 Expressions of the voltage and current for the HF injection network

The frequency of the link current and the HF injected current is the same. In the positive cycle of the link current, the HF injected current decreases from its positive peak to negative peak and in the negative cycle of the link current,

the HF injected current increases from its negative peak to positive peak. The instantaneous current through the HF current injection branch of the *R* phase is expressed in equation (25), using a Fourier series. Expressions for the instantaneous current through the HF current injection branch and the voltage across L_f and C_f of the other two phases can be written using equations (25) to (28).

$$i_{LfR} = \sum_{n=1,3,5,7.....}^{\infty} \frac{8I_{Lfp}}{n^2\pi^2} \cdot \left(1 - \cos\left(\frac{n\pi}{2}\right)\right) \cdot \cos\left(n\omega_s t\right)$$

$$i_{CfR} = i_{LfR} \qquad (25)$$

where I_{Lfp} is the peak value of i_{LfR}. This value varies over the cycle of the input supply voltage. The I_{Lfp} is equal to I_m at the peak of the input supply voltage (Fig 2(a)). Equations (13) and (16) give the value of I_{Lfp} as

$$I_{Lfp} = \frac{2}{3}\frac{P_o}{\eta.V_m}\sin\omega t \qquad (26)$$

The instantaneous voltages across L_f and C_f of the HF current injection branch of phase R are given by,

$$v_{LfR} = \sum_{n=1,3,5,.....}^{\infty} \frac{8I_{Lfp} \cdot X_{Lfn}}{n^2\pi^2}\left(1 - \cos\left(\frac{n\pi}{2}\right)\right)\sin\left(n\omega_s t\right) \qquad (27)$$

$$v_{CfR} = -\sum_{n=1,3,5,7.....}^{\infty} \frac{8I_{Lfp} \cdot X_{Cfn}}{n^2\pi^2}\left(1 - \cos\left(\frac{n\pi}{2}\right)\right)\sin\left(n\omega_s t\right) \qquad (28)$$

To find the VA stresses on the reactive elements the equations for the link current (20) and the HF injected current (25) are used. The total kVA/kW rating of the converter is calculated using these VA stresses. The variation of kVA/kW with respect to normalized switching frequency (ω_s/ω_r) is studied and plotted in Fig. 4(a) for various values of quality factor *Q*. It shows that kVA/kW decreases with an increase in switching frequency. The kVA/kW depends on the quality factor *Q* and it decreases with decreases in *Q*.

3.3 Turn off stresses of the switching devices of the HF inverter

The instantaneous current through the switching device (i_{switch}) of the HF inverter is the instantaneous sum of the link current and the HF injected current.

$$i_{switch} = i_{link} - i_{Lf} \qquad (29)$$

To determine i_{switch} (using (20) and (25)), only the fundamental component of the link current is used. Since the converter is operated at above resonance frequency, the link current lags the respective phase voltage by θ_{eq}. As the frequency of the HF injected current and the link current become equal, from Fig. 2(b) it is clear that the HF injected current also shifts through the same phase angle θ_{eq} on the time axis. Hence, applying the shifting of time reference theorem to the Fourier series of the HF injected current, i_{Lf} is written in (30). The duty ratio *d* is maintained constant throughout the loading conditions, where $d = 50\%$. Hence, $\delta = \pi$ rad. For leg 'a' of the HF inverter,

$$i_{switcha} = \frac{2V_{rect}}{\pi\left|Z_{eq}\right|} \cdot \sin\left(\omega_s t - \theta_{eq}\right) - \sum_{n=1,3,5,7.....}^{\infty} \frac{8I_{Lfp}}{n^2\pi^2} \cdot \left(1 - \cos\left(\frac{n\pi}{2}\right)\right) \cdot \cos\ n\left(\omega_s t - \theta_{eq}\right)$$

when $i_{s1} = i_{switcha}$ $(0 \le \omega_s t \le \pi)$ and $i_{s4} = i_{switcha}$ when $(\pi \le \omega_s t \le 2\pi)$ (30)

Similarly, using equations for the link current and the HF injected current for phases *Y* ($i_{switchb}$) and *B* ($i_{switchc}$) can be obtained with the phase shift of 120^0.

$i_{s3} = i_{swichb}$ when $(0 \le \omega_s t \le \pi)$ and $i_{s6} = i_{switchb}$ when $(\pi \le \omega_s t \le 2\pi)$ (31)

$i_{s5} = i_{switchc}$ when $(0 \le \omega_s t \le \pi)$ and $i_{s2} = i_{switchc}$ when $(\pi \le \omega_s t \le 2\pi)$ (32)

Due to ZVS, the turn-on stresses of the switching device are reduced to zero. Connecting a loss-less snubber across the switching devices reduces the turn-off stresses of the switching devices. In this section the turn-off stresses are also calculated. The turn-on current of S_1 is equal to the turn-off current of S_4. Similarly, the turn-on current of S_3 is equal to the turn-off current of S_6 and the turn-on current of S_5 is equal to the turn-off current of S_2.

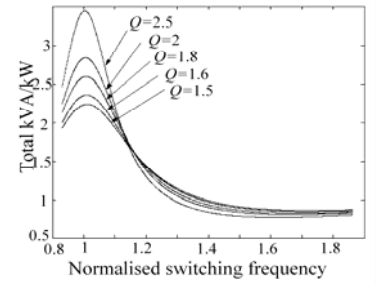

(a)

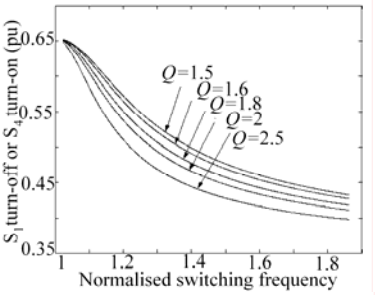

(b)

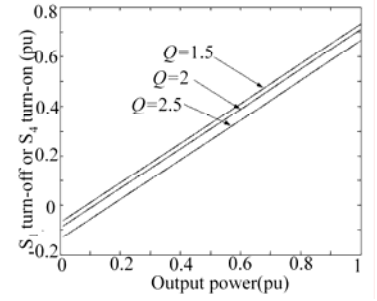

(c)

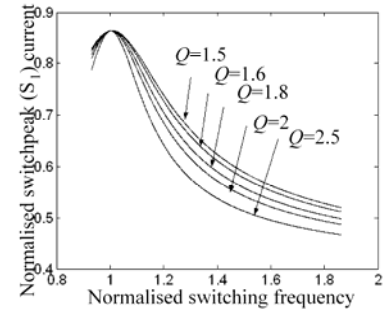

(d)

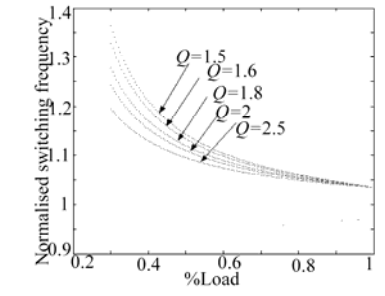

(e)

Fig. 4 Design curves (a) plot of kVA/kW against normalised switching frequency (Y_s) (b) Variation of turn-off stress of S_1 with Y_s (c) Variation of turn-off stress of S_1 with the P_o (d) Variation of $i_{switchp}$ of S_1 with Y_s (e) Variation of Y_s required to regulate the V_o under different loading conditions

Hence, at $\omega_s t = \pi$, equations (30) to (32) give the turn-off stresses of S_1, S_3 and S_5, respectively. Where as at $\omega_s t = 2\pi$, equations (30) to (32) give the turn-off stresses of S_4, S_6 and S_2, respectively. The variation of normalized stress with respect to the normalized switching frequency is studied for all six switching devices of the HF inverter. Turn off stress is reduced by an increase in switching frequency or an increase in quality factor Q. The turn-off stress is highest at the full load and at the peak of the input supply. The variation of the turn-off stresses with respect to the normalized switching frequency is plotted in Fig. 4(b) for various values of quality factor Q. This shows that as the switching frequency increases, stress decreases. Similarly, with an increasing value of Q, stress decreases. Fig. 4(c) shows the variation of the turn-off stress with respect to the output power for various values of quality factor Q. It shows a decrease in stress with a decrease in output-power at resonance frequency.

3.4 Calculation of the switch peak current

The rms current through the switch S_1 can be derived from equation (30),

$$I_{S1rms} = \sqrt{\frac{1}{2\pi}\cdot\left(\int_0^{\pi}\frac{2V_{rect}}{\pi|Z_{eq}|}\cdot\sin\left(\omega_s t-\theta_{eq}\right)-M\right)^2 d\omega_s t}$$

where,

$$M = \sum_{n=1,3,5,7.....}^{\infty}\frac{8I_{Lfp}}{n^2\pi^2}\cdot\left(1-\cos\left(\frac{n\pi}{2}\right)\right)\cdot\cos\left(n\omega_s t-\theta_{eq}\right)$$

$$I_{S1peak} = \sqrt{2}I_{S1rms} \qquad (33)$$

Similarly, using equations (30) to (32), the rms and the peak current conducted by the switches S_2 to S_6 can be derived. The peak value of the HF injected current varies over the time period of the input supply. It has maximum value at the peak of the input supply. Variation of the normalized switch peak current with respect to the normalized switching frequency at the peak of the input supply is studied and plotted in Fig. 4(d) for various values of the quality factor Q and at full load. The switch peak current reduces with an increase in switching frequency or quality factor Q.

This suggests selection of a higher value of the quality factor to reduce the switch peak current. The volt-ampere rating of the switch is given by,

$$Switch\ VA\ rating = V_{rect} \cdot I_{Speak} \quad (34)$$

The design curves plotted in this section give guidelines for designing MSPRC components, HF current injection network components and for selecting switching devices of the HF inverter.

4. Design of the Converter

In this section the design of the proposed three-phase ac-to-dc resonant converter operating in high power factor mode for a high-voltage dc application is outlined. The specifications of the proposed converter are as follows:

4.1 Specifications of the three-phase ac-to-dc resonant converter

The ac input phase voltage, $V = 115$ V, 50 Hz

Output DC voltage, $V_0 = 1000\ V$

Output Power, $P_0 = 3$ kW

Resonant frequency, $f_r = 290$ kHz

Minimum switching frequency, $f_s = 300$ kHz

Selecting the following base values;

$V_{base} = V_{LL} \cong 200\ V = 1\ pu,\ P_{base} = P_0 = 3\ kW = 1\ pu$

$\omega_{base} = \omega_r = 1\ pu, I_{base} = P_{base}/V_{base} = 15\ A,$

$I_{base} = P_{base}/V_{base} = 15\ A,\ Z_{base} = V_{base}/I_{base} = 13.33\ \Omega,$

$L_{base} = Z_{base}/\omega_{base} = 7.31\mu H,\ C_{base} = 1/(Z_{base} \cdot \omega_{base}) = 41.17$

4.2 Output current and inverter output voltage

Output current, $I_0 = P_0/V_o = 3 = 0.2\ pu$

Load Resistance, $R_L = V_0/I_0 = 333.33\Omega = 25\ pu$. From (9) and (19) the rms value of the fundamental component of the HF inverter phase voltage, $V_{rms1} = \frac{\sqrt{2}}{\pi} V_{rectpu} = 0.727\ pu$

4.3 HF Transformation ratio

- From (22), $V_{primpu} = \frac{\sqrt{2}}{\pi} V_{rectpu} = 0.727\ pu$.
- To obtain the output voltage of 1000 V, the average output voltage of each single–phase diode bridge rectifier should be 333.33 V. The rms value of the voltage at the input terminal of single-phase HF diode bridge rectifier, i.e. at the secondary of the HF transformer, is required to be, $V_{\sec} = (333\,\pi)/(2\sqrt{2}) = 369 = 1.84\ pu$.
- Transformation ratio, $N_1 : N_2 = n_t = 0.727 : 1.84 \approx 12 : 31$

4.4 Design of the MSPRC tank circuit

The output voltage of the converter is regulated by the variable frequency control (fixed duty ratio) method keeping the input voltage constant. Fig. 4(e) shows the variation in switching frequency required to regulate the output voltage for various values of quality factor *Q*. It reveals that a narrow variation in switching frequency is required to regulate the output voltage for lower values of *Q*. Hence, after studying Fig. 4(a) to 4(e), Q =1.8 is selected. Using the design procedure given in [7], the resonant components values are calculated. The values of the reactive components of the tank circuit are obtained as,

$L_1 = 50.58\mu H = 6.92\ pu, C_1 = 6.55nF = 0.159 pu, L_2 = 505.8\mu H = 69.2\ pu,$
$C_2 = 65.5nF = 1.59 pu, C_p = 0.655nF = 0.0159\ pu, C_p' = 4.3nF = 0.104\ pu.$

4.5 Design of feedback branch element

Assuming that the efficiency $\eta = 92\%$ for the converter, equation (17) gives $L_f = 10.03\mu H = 1.37\ pu.$ At the peak of the input supply voltage, the peak of the injected current is equal to the maximum input line current (I_m). Hence, L_f should be designed so that it will carry the maximum input line current safely. Magnetic components of the proposed converters (including L_1 and L_2 in the tank circuit, the HF transformer, the filter inductance L_d and the HF current injected inductor L_f) need to be designed to minimize the core and winding losses. The ferrite materials provide very high volume resistivity, which minimizes the eddy current losses. Hence, the ferrite cores are selected. To reduce the copper loss in winding at high frequency due to the skin effect, litz wire is used. The capacitor C_f provides dc blocking for the HF injected current, therefore C_f should be sufficiently large enough so that it has a constant voltage over the switching cycle depending upon the duty ratio. Since the duty ratio is maintained at 50%, $V_{Cf} = V_{rect}/2$. $C_f = 1\mu F$ is selected.

4.6 Design of the output filter components

The output dc voltage of the converter has harmonics. This voltage has a ripple frequency six times the minimum inverter switching frequency. The rms value of each harmonic is given by,

$$V_{rn} = \frac{2 \cdot V_0}{4 \cdot n^2 - 1} \tag{35}$$

where n is a multiple of $2f_s$. The 6th harmonic is dominant and its rms value is given by, $V_{r3} = 2 \cdot V_0 / 35$. The value of the filter inductance is calculated using the peak-to-peak ripple specification of the output current (I_{p-p}) as below.

$$L_d = \frac{2(2V_o/35)}{6\omega_s I_{p-p}} = \frac{V_o}{105\,\pi\, f_s I_{p-p}} \tag{36}$$

The value of the output filter capacitor needed for the specified peak-to-peak ripple specification of the output voltage is calculated as follows. The magnitudes of the harmonic components of the rectified output current are given by,

$$I_{rn} = \frac{2\ I_o}{4\ n^2 - 1} \tag{37}$$

The sixth harmonic is dominant; the rms value of this component is given by, $I_{r3} = 2 \cdot I_0 / 35$. The output filter capacitance C_d, which is required to limit the six times line frequency (f) component of the rectifier output voltage to the ripple specification V_{p-p} is determined by,

$$C_d = \frac{2(2\ I_o/35)}{6\ \omega\ V_{p-p}} = \frac{I_o}{105\ \pi\ f\ V_{p-p}} \tag{38}$$

For $I_{p-p} = \pm 5\%$ of I_0 and $V_{p-p} = \pm 10\%$ of V_o, L_d = 33.68μH, C_d = 1.03 μF.

5. Results

In this section, the experimental results of the 3 kW, 1000 V laboratory set up of the three-phase ac-to-dc resonant converter are presented. To verify the theoretical performance and design procedure of the converter, the circuit is simulated using 'PSIM'. The operating waveforms shown in Fig. 2 are studied and verified at the peak as well as at the valley point of the supply voltage. An experimental prototype is fabricated, using HF diodes $DSEI\ 60-12\ A$, and IGBTs $HGTG\ 20N60A4D$. The resonant magnetic components, feedback inductor, and output filter inductor are built using a ferrite core and litz wire. The output voltage of the converter is regulated by varying the frequency of the HF inverter. A DSP $(TMS320F2812)$ program is developed to control the switching frequency of the three-phase HF inverter. For the experimental prototype, the following actual values of components are selected.

$L_s = 0.5mH,\ C_{rect} = 10\mu F,\ L_1 = 50\,\mu H, C_1 = 6.5nF, L_2 = 500\mu H,$
$C_2 = 65nF, C_p' = 4.7nF,\ L_f = 10\mu H, C_f = 1\mu F, L_d = 33\mu H, C_d = 2.5\mu F$

. Fig. 5 shows the waveforms of the input voltage, input current at full load, 50% load and 25% load. The line current total harmonic distortion (THD) is studied. The full load THD is 3.1% and the efficiency is 92%. From FFT analysis (Fig. 5(d)) it is clear that the amount of fifth harmonic current is significantly reduced. The line current THD at 25% load is 11%. From the experimental waveforms it can be seen that the proposed converter has high power factor throughout the loading conditions. The HF modulated input voltage of the diode bridge rectifier v_R' for *R*-phase is shown in Fig. 6(a). The output voltage of the input diode bridge rectifier, i.e. the voltage across $C_{rect,}$ is shown in Fig. 6(b). V_{rect} has low frequency ripples of 300 Hz as C_{rect} is very small. With the selected value of L_s, the phase angle of the fundamental component of v_R' is, $\alpha = \tan^{-1}(V_{Ls}/V_R) = 0.77^0$. The instantaneous voltage and current waveforms for the HF full bridge inverter at full load condition are shown in Fig. 7. Here, the instantaneous values of the phase voltages along with the link currents are shown. Fig. 7(b) shows the ZVS operation of the converter.

From these waveforms, it can be noted that at the instant of turn-on of the switch, the voltage across the switch is almost equal to zero. Therefore, all the switching devices are turned-on with ZVS. This eliminates the turn-on losses. Fig. 8 gives the experimentally obtained current and voltage across the HF current injection inductor. It was observed that the switch peak current and injected current decreased with the load maintaining high partial load efficiency. The output voltage and current are shown in Fig. 9.

Table 1 shows the performance characteristics converter.

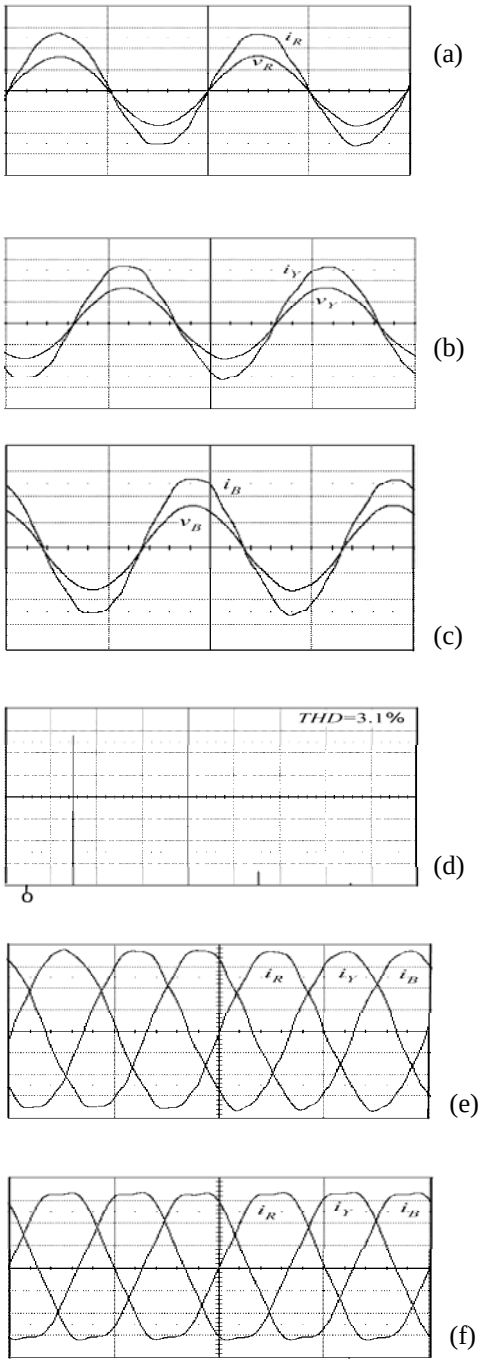

Fig. 5 Experimental waveforms of input voltage and input current at full load. (a) phase R, (b) phase Y, (c) phase B. Scale: Time 10 ms/div. Voltage: 100 V/div. Current 5 Amp/div. (d) FFT of Phase R current at full load, Scale X axis: 50 Hz/div. Y axis: Current 2 Amp/div. (e) Waveforms of input currents at 50% load, current scale: 2 Amp/div. (f) Waveforms of input currents at 25% load, current scale: 1 Amp/div

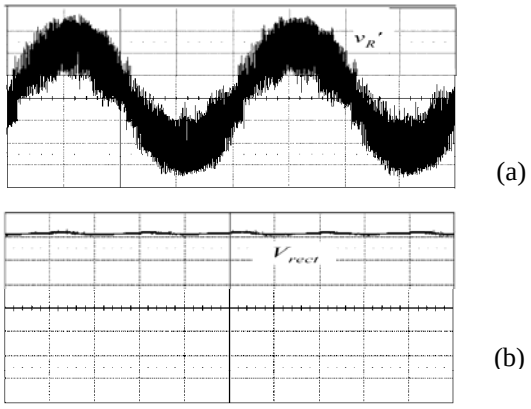

Fig. 6 Experimental waveforms of input and output voltage of the input diode bridge rectifier at me 2ms/div. Voltage: 100 V/div

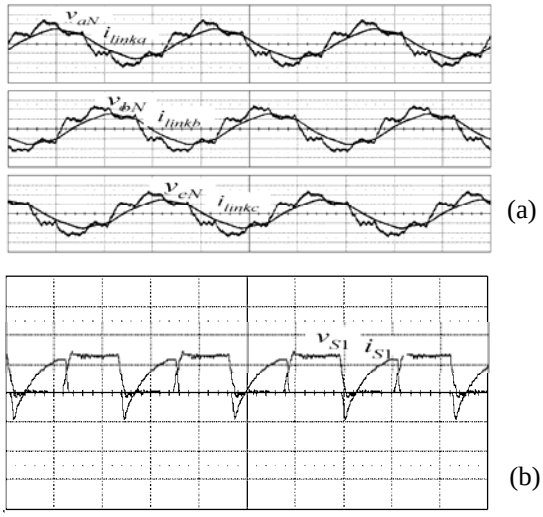

Fig. 7 Experimental waveforms of voltage and current of the three-phase HF inverter at full load. Scale: Time 1μs/div. (a) Output phase voltage and link current of three phases a, b, c Voltage: 100V/div., Current 10 Amp/div. (b) Voltage across switch S_1 and current through S_1, Voltage: 200V/div. Current 10 Amp/div

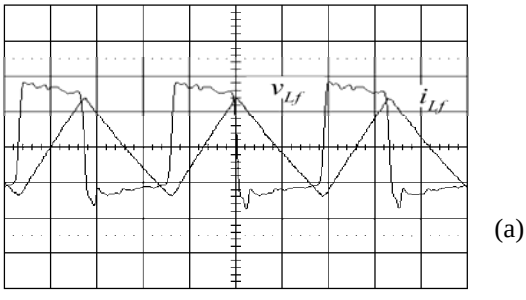

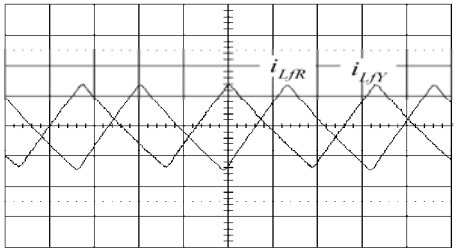

(b)

Fig. 8 Experimental waveforms of voltage and current of HF current injection inductor L_f at full load. Scale: Time 1μs/div., Current 10 Amp/div., Voltage 100 V/div. (a) Voltage across L_f and current through L_f (b) Current through L_f of Phases R and Y

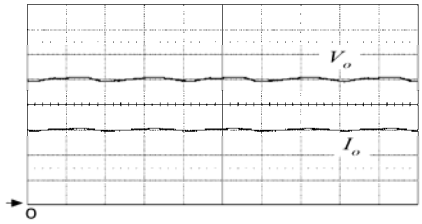

Fig. 9 Experimental waveforms of output voltage and output current of the converter at full load. Time scale 2 ms/div., Current 1 Amp/div., Voltage 200 V/div

Table 1 Performance of the converter

Percentage of load	Full load	50% load	25% load
Frequency required	300 kHz	351 kHz	372 kHz
THD	3.1%	4.2%	11%
Power factor	0.99	0.99	0.98
Efficiency	0.92	0.93	0.89

6. Conclusion

In this paper, an analysis of a three-phase ac-to-dc resonant converter with high input power factor and isolated output is presented. To improve the input power factor of the converter, high frequency current is injected into the input of the diode bridge rectifier. The operation of the converter is analyzed. To study the relationship and variation of the parameters, MATLAB subroutines are developed and different design curves are plotted. The design example is summarized along with the component ratings.

Since the high frequency switches are turned on under ZVS, the converter has less losses and high efficiency. To reduce voltage stresses and switching and conduction losses in the diodes of the output bridge rectifier, three single-phase diode bridge rectifiers are connected in series at the output HF transformer. The concept presented in the paper is verified by simulation using the 'PSIM' package. Finally, to verify the theoretical and simulated performance of the converter, experimental results from laboratory tests on a prototype of 3 kW, 1000V output, operating above 300 kHz are provided. The input currents of the converter have practically sinusoidal waveforms for large variations of the load resistor. The proposed three-phase ac-to-dc resonant converter requires narrow variation in switching frequency to regulate the output voltage from full load to 25% load.

References

[1] Chin S. Moo, Ching R. Lee, and Tsai F. Lin, " A high power factor dc linked resonant converter", *IEEE transactions on Industry Electronics*, Vol. 46, No. 4, pp 814-819, August 1999.

[2] H. M. Suryawanshi, K. L. Thakre, S. G. Tarnekar, D. P. Kothari, and A. G. Kothari "Power factor improvement and closed loop control of an ac-to-dc resonant converter," *IEE Proc.-Electr. Power Applications*, Vol. 149, No.2, pp. 101-110, March 2002.

[3] H. M. Suryawanshi, K. L. Thakre, S. G. Tarnekar, D. P. Kothari, and A. G. Kothari "Power factor improvement and closed loop control of an ac-to-dc resonant converter," *IEE Proc.-Electr. Power Applications*, Vol. 149, No.2, pp. 101-110, March 2002.

[4] A.K.S. Bhat, and R. L. Zheng, "A three-phase series–parallel resonant converter–Analysis, design, simulation, and experimental results," *IEEE transactions on Industry Electronics*, Vol. 32, No. 4, pp 951-961, August 1996.

[5] A.R. Prasad, P. D. Zigas, and S. Manias, "A three-phase resonant PWM DC-DC converterer," *PESC* 1991, pp.463-472.

[6] F.S. Hamdad, and A.K.S. Bhat, "Three-phase single stage ac/dc boost integrated parallel resonant converter," *IEEE transactions on Aerospace and Electronic Systems*, Vol. 40, No. 4, pp 1311-1323, Oct. 2004.

[7] S. S. Tanavade, H. M. Suryawanshi, and K. L. Thakre, "Novel single-phase AC-to DC converter using

three-phase modified series-parallel resonant converter," *IEE Proc.-Electr. Power Applications*, Vol. 152, No.4, July 2005.

[8] M. Rastogi, R. Naik, and N. Mohan, "Optimization of novel dc link current modulated interface with three-phase utility system to minimise line current harmonics,"*PESC*, 1992, vol. 1, pp. 162–167.

[9] Predrag Pejovic, "An Analysis of Three-Phase Low –Harmonic Rectifiers Applying the Third–Harmonic Current Injection," *IEEE transactions on Power Electronics*, Vol. 14, No. 3, pp 397-407, May 1999.

[10] Sikyung Kim, and Prasad N. Enjeti, "A new approach to improve power factor and reduce harmonics in a three-phase diode rectifier type utility interface," *IEEE transactions on Industry Applications*, Vol.30, No. 6, pp 1557-1563, Dec.1997

[11] Andrew M. Cross, and Andrew J. Forsyth, "A High-Power-Factor, Three-Phase Isolated AC–DC Converter Using High-Frequency Current Injection," *IEEE transactions on Power Electronics*, Vol. 18, No. 4, pp 1012-1019, July 2003.

[12] J.A.M.Bleijis, "Continuous conduction mode operation of three-phase diode bridge rectifier with constant load voltage," *IEE Proc.-Electr. Power Applications*, Vol. 152, No.2, pp.359-368, March 2005.

[13] Prasad N. Enjeti, and Ashek Rahman, " A new single-phase to three-phase converter with active input current shaping for low cost ac motor drives," *IEEE transactions on Industry applications, vol. 29, no. 4, July/August 1993, pp. 806-813.*

[14] N. Mohan, T. Undeland, and W.Robbins, "Power Electronics Converters, Applications, and Design," *3rd edition* 2003, *John Wiley and Sons*.

[15] Y. Zhongming, P. Jain, and P. Sen, "A high efficiency high frequency resonant inverter for high frequency ac power distribution architectures," 37 th *IEEE PESC conference, June 2006, pp. 958-964.*

Madhuri A. Chaudhari was born in Maharashtra, India on 28th January 1968. She received her B.E., M. Tech., and Ph.D. degrees in Electrical Engineering from Amaravati University, V.R.C.E.- Nagpur University and V. N. I. T. Nagpur respectively. She is working as a Professor with the Electrical Engineering department of Yeshwantrao Chavan College of Engineering Nagpur. Her research interests are in the areas of power electronics, FACTS, and AC-DC drives. She is a member of the Institution of Engineers (India) and I. S.T.E.

Hiralal M. Suryawanshi (M'06) was born in Nagpur, India, on January 1, 1963. He received the B. E. degree in Electrical Engineering from Walchand College of Engineering, Sangli, India, in 1988 and the M. E. degree in Electrical Engineering from the Indian Institute of Science, Bangalore, in 1994. He was awarded the Ph. D. degree by Nagpur University, Nagpur (India) in 1998. He is a member of IEEE, IEE and MIE(I). He is currently working as an Assistant Professor in the Department of Electrical Engineering, Visvesvaraya National Institute of Technology, Nagpur, (India). His research interests include the field of power electronics, emphasising developmental work in the area of resonant converters, power factor correctors, active power filters, FACTs devices, multilevel converters and electric drives.

Abhishek Kulwal was born on 17th September 1981 received a Bachelor's Degree in Electrical Engineering from Nagpur University in 2003 and completed a Master's in Integrated Power Systems (IPS) from Visvesvaraya National Institute of Technology, Nagpur, India in 2006. His areas of interest are power electronics based high power converters and adjustable speed drives.

Mahesh K. Mishra (S'00–M'01) received the B.Tech. degree from the College of Technology, Pantnagar, India, in 1991, the M.E. degree from the University of Roorkee, Roorkee, India, in 1993, and the Ph.D. degree in Electrical Engineering from the Indian Institute of Technology, Kanpur, India, in 2002. Currently, he is an Assistant Professor in the Electrical Engineering Department with the Indian Institute of Technology, Madras, Chennai, India. His interests are in the areas of power electronics, power system, and controls.